# High-resolution two-photon spectroscopy of rubidium within a confined geometry

C. Perrella,[1] P. S. Light,[1] J. D. Anstie,[1] T. M. Stace,[2] F. Benabid,[3] and A. N. Luiten[1,4]
[1]*School of Physics, University of Western Australia, Perth, Western Australia 6009, Australia*
[2]*Department of Physics, University of Queensland, Brisbane, Queensland 4072, Australia*
[3]*Xlim Research Institute CNRS, University of Limoges, Limoges, France*
[4]*Institute of Photonics and Advanced Sensing (IPAS) and the School of Chemistry and Physics, The University of Adelaide, Adelaide SA 5005, Australia*
(Received 14 September 2012; published 17 January 2013)

We present two-photon spectroscopy of a thermal rubidium vapor confined to the hollow core of a photonic-crystal fiber. Linewidths as narrow as 10 MHz were observed on the $5S_{1/2} \rightarrow 5D_{5/2}$ transition enabling the hyperfine splitting of the excited state to be resolved. Very strong nonlinear absorption (>90%) was observed, with substantial absorption maintained over large detunings (9 GHz) from an intermediate state. These attributes make this system ideal for many frequency metrology and quantum optics applications.

DOI: 10.1103/PhysRevA.87.013818 PACS number(s): 42.81.Qb, 32.30.−r, 78.47.da, 78.47.N−

## I. INTRODUCTION

Atomic transitions involving the absorption of two photons [1] offer a platform for all-optical switches [2–4], single-photon generation [5], photon coherence measurements, and quantum logic gates [6,7], due to their ability to modulate, or sense, one light field with another. Such transitions also offer narrow linewidths beneficial for frequency metrology applications such as atomic clocks and frequency stabilization [8,9]. For these applications, nonlinear transitions are most useful when they deliver strong absorption at low optical powers. This characteristic has previously been demonstrated using resonant enhancement through an intermediate energy level together with strongly focusing optics [1,10]. Here, we extend this concept by utilizing the technology of hollow-core photonic-crystal fibers (HC-PCF) [11,12], which can deliver high optical intensities for low input powers. Furthermore, the fiber maintains tight overlap of the highly confined optical mode and atomic vapor over arbitrary lengths.

Three key properties determine the performance of two-photon transitions in the aforementioned applications: the ultimate absorption strength, the absorption linewidth, and the range of frequency detunings, from the intermediate state, over which it is possible to maintain these properties. In this paper we explore these performance criteria for the $5S_{1/2} \rightarrow 5D_{5/2}$ two-photon transition of rubidium (Rb) [13,14] loaded into a HC-PCF. This system was chosen for its potentially narrow linewidth and strong absorption, which was further enhanced by driving the transition in near resonance with the $5S_{1/2} \rightarrow 5P_{3/2}$ single-photon transition.

## II. SETUP

Two lasers, of wavelengths 780 and 776 nm, drove the $5S_{1/2} \rightarrow 5D_{5/2}$ two-photon transition as shown in Fig. 1(a). Specifically, we focus on the $^{87}$Rb $5S_{1/2}$ $(F = 2) \rightarrow 5D_{5/2}$ $(F' = 1–4)$ set of transitions for the majority of this paper. From the excited state, Rb can decay to the ground state through either the original intermediate state, or via the $6P_{3/2}$ energy level, which emits 420 nm fluorescence on decay back to the ground state [see Fig. 1(a)]. For the rest of this paper, the ground $(5S_{1/2})$ state will be labeled $|g\rangle$, while the intermediate $(5P_{3/2})$ and excited $(5D_{5/2})$ energy levels will be labeled $|i\rangle$ and $|e\rangle$, respectively, with natural linewidths $\gamma_i$ and $\gamma_e$. Detunings from these states will be labeled $\Delta_i = \omega_{gi} - \omega_{780}$ and $\Delta_e = \omega_{gi} + \omega_{ie} - (\omega_{780} + \omega_{776})$, where $\omega_{jk}$ denotes the $|j\rangle \rightarrow |k\rangle$ transition frequency. The optical power coupling energy levels $|j\rangle$ and $|k\rangle$ will be denoted as $P_{jk}$.

The fiber used in this work was kagome-structured HC-PCF [15], with core diameter 45 $\mu$m providing low-loss guidance from 1600 to 600 nm [the fiber's cross section is shown in Fig. 1(b)]. Each end of the fiber was held within separate vacuum chambers, only one of which was loaded with Rb, while the midsection was outside the vacuum. The fiber was curved between the vacuum chambers, which, combined with its large core diameter, resulted in coupling to higher-order transverse optical modes. The Rb vapor density within the fiber was controlled by adjusting the temperature

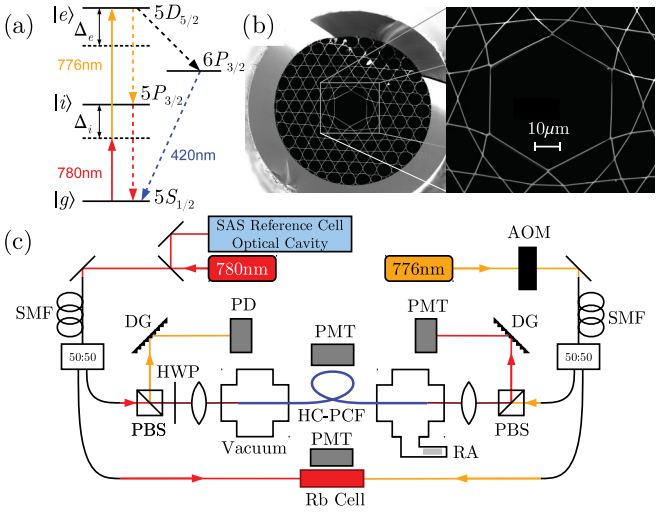


FIG. 1. (Color online) (a) Two-photon transition energy level diagram. Solid arrows are driving lasers; dashed arrows show decay routes. (b) Scanning electron microscope image of the kagome HC-PCF used. (c) Schematic of the optical experimental setup. AOM, acousto optic modulator; SMF, single mode fiber; HWP, half wave plate; PBS, polarizing beam splitter; DG, diffraction grating; PMT, photomultiplier tube; PD, photodiode; and RA, rubidium ampoule.

 

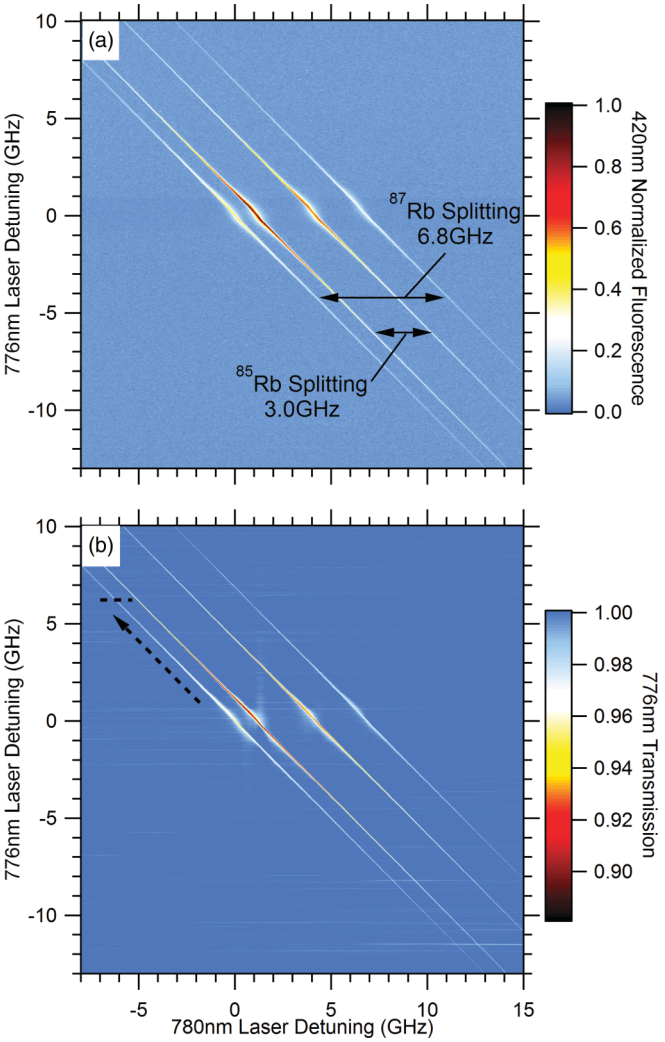


FIG. 2. (Color online) Frequency map of the $|g\rangle \rightarrow |e\rangle$ transition. Map (a) shows 420 nm fluorescence. Hyperfine ground-state splittings are highlighted. Map (b) shows 776 nm absorption. The dashed line and arrow depict how the data presented in Figs. 3 and 4, respectively, was analyzed. Laser powers were $P_{gi} \approx 90\ \mu$W and $P_{ie} \approx 200\ \mu$W.

of the fiber and vacuum chamber, nominally kept at 90 °C for the reported experiments. Fluorescence measurements probed the Rb density within the fiber showing over half the 40-cm fiber was loaded. Furthermore, the Rb density was observed to decrease along the fiber's length away from the loading chamber. Nonetheless, pressure broadening and line shifts ($\approx$12 kHz [8,16,17]) for the largest vapor densities ($\approx 2 \times 10^{18}$ m$^{-3}$ [18]) are below the resolution of this experiment.

The optical setup used to excite the two-photon transition is shown in Fig. 1(c). This consisted of two tunable lasers: an extended cavity diode laser (ECDL) at $\sim$780 nm and a Ti:sapphire laser at $\sim$776 nm. For high-resolution measurements, laser noise was minimized by stabilizing the ECDL to a reference optical cavity yielding a beat note between the Ti:sapphire and ECDL with a full width at half maximum (FWHM) of $<$300 kHz. The 776-nm laser passed through an acousto optic modulator to provide power control. Both lasers passed through single mode fibers, before their polarizations were set to be orthogonal. Two 60-mm lenses then coupled each laser into the HC-PCF from either end to allow Doppler-free spectroscopy of the two-photon transition. Optical powers $P_{gi}$ and $P_{ie}$ were measured after the fiber so that optical in-coupling losses into the fiber were included. We simultaneously observed 420 nm fluorescence and absorption of both excitation beams using photomultiplier tubes and a photodiode with suitable dichroic filters.

The two-photon transition was also excited within a room temperature bulk Rb cell, in order to compare the characteristics of the fiber and bulk cell systems. Both lasers had a $1/e^2$ waist diameter of $\approx$1.3 mm with typical laser powers of $P_{gi} \approx 1$ mW and $P_{ie} \approx 20$ mW. These powers were sufficiently low to avoid saturation effects. A mu-metal shield reduced magnetic fields inside the cell below the resolution of the experiment. The temperature of the cell was 22 °C, which corresponded to a vapor density of $\approx 7 \times 10^{15}$ m$^{-3}$ [18].

The frequency of the Ti:sapphire laser was measured using a wave meter with a relative accuracy of 5 MHz. The ECDL's frequency was measured using a combination of an optical cavity, providing equispaced frequency markers (300 MHz), and the saturated absorption features from a Rb reference cell, providing an absolute frequency reference. This procedure provided a frequency scale with an estimated accuracy of 2 MHz.

## III. TWO-DIMENSIONAL MAPS

The two-dimensional maps in Fig. 2 show the dependence of the two-photon transition strength on detunings from both the intermediate and excited state transitions. This was achieved by scanning both lasers to completely explore a 23 $\times$ 23 GHz two-dimensional frequency detuning space centered on the single- and two-photon transitions while detecting both the 420 nm fluorescence [Fig. 2(a)] and 776-nm absorption [Fig. 2(b)]. The 780-nm absorption map is complicated by single-photon absorption features, and hence, is not shown. However, when well detuned from single-photon resonance ($|\Delta_i| \gg 900$ MHz), and in two-photon resonance, the 780-nm beam typically displayed stronger absorption than the 776-nm beam due to its larger dipole moment. Hence, the rest of this paper presents absorption of the 780-nm beam while in two-photon resonance. We will term this 780-nm absorption as the two-photon absorption for the remainder of this paper.

The four strong diagonal lines apparent in both panels of Fig. 2 represent the two-photon Doppler-free transition between the ground and excited states. Each isotope of Rb contributes two lines due to ground-state hyperfine splitting, with the two central lines belonging to $^{85}$Rb, and the outer two to $^{87}$Rb. These lines have a measured gradient of $-1.0000(1)$, and hence map out a diagonal line of constant sum frequency corresponding to $\Delta_e = 0$.

Each of the four main absorption features in Figs. 2(a) and 2(b) consist of multiple absorption lines originating from excited state hyperfine splitting. These lines are not visible in Fig. 2 due to their narrow frequency spacing, but are readily resolved in our setup. A spectra taken through one of the main absorption lines [depicted by the horizontal dashed line in Fig. 2(b)] reveals the excited state hyperfine splitting, shown in Fig. 3 for both the HC-PCF and reference cell. Theoretical analysis of the two-photon transition [1,10] shows the spectral

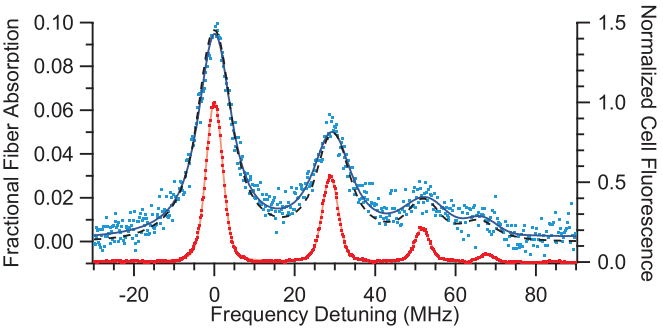


FIG. 3. (Color online) Two-photon absorption as a function of two-photon detuning $\Delta_e$ of the fiber (blue, upper) and cell (red, lower). Also shown are fits to Eq. (1) and a theoretical line shape (black dashed) discussed in Sec. V.

lineshape takes the form of a Voigt profile:

$$\alpha(\Delta_e) \propto \int_{-\infty}^{\infty} \frac{e^{-(\Delta_z/\gamma_{\mathrm{RD}})^2}}{4(\Delta_e - \Delta_z)^2 + \gamma_e^2} d\Delta_z. \tag{1}$$

The Gaussian component of the Voigt profile arises from residual Doppler broadening as the two counterpropagating laser frequencies are not identical [1]. The fiber and cell give residual Doppler broadenings of $\gamma_{\mathrm{RD}} = 1.9$ and 1.7 MHz, respectively, with the variation due to different operating temperatures (90 °C and 22 °C, respectively). The Lorentzian component arises from the $|g\rangle \rightarrow |e\rangle$ transition line shape with a natural FWHM of 667 kHz (lifetime of 238 ns [19]) which can be power broadened. The optical depth observed in the $|g\rangle \rightarrow |i\rangle$, 780-nm coupling laser, $\alpha(\Delta_e)$, is related to observed absorption via $\mathscr{A}(\Delta_e) = 1 - e^{-\alpha(\Delta_e)}$ and the two-photon transition rate $w(\Delta_e)$ by $\alpha(\Delta_e) \propto w(\Delta_e)/P_{gi}$. Equation (1) was fitted to the retrieved spectra, as shown in Fig. 3, with no fixed fitting parameters. The individual Lorentzian and Gaussian widths could not be extracted as the signal-to-noise ratio of the data was not sufficient to retrieve both values reliably. However, the FWHM of the Voigt consistently returned reliable values, which are presented here. These fits allowed the amplitude, linewidth, and excitation bandwidth of this transition to be investigated along with their dependence on experimental parameters such as laser powers and detuning from the intermediate level.

## IV. TWO-PHOTON CHARACTERISTICS

The two-photon absorption as a function of detuning from the intermediate state is shown in Fig. 4(a). This data corresponds to tracking along the absorption line, depicted by the dashed diagonal arrow on the 2D map in Fig. 2(b) (i.e., $\Delta_e = 0$), by postprocessing 780-nm absorption spectra similar to Fig. 3 for varying $\Delta_i$. For large detunings, of up to 9 GHz, significant absorption (>10%) is still observed. Stepwise excitation through $|i\rangle$ is negligible in Fig. 4 as $|\Delta_i| \gg \gamma_{\mathrm{Dop}}/2$, where $\gamma_{\mathrm{Dop}} \approx 1.8$ GHz is the Doppler-broadened FWHM of the intermediate state. In this limit, the resonant two-photon transition rate $w(0)$ for a stationary atom in a low-power laser field (where the absorption is power independent [20]) depends

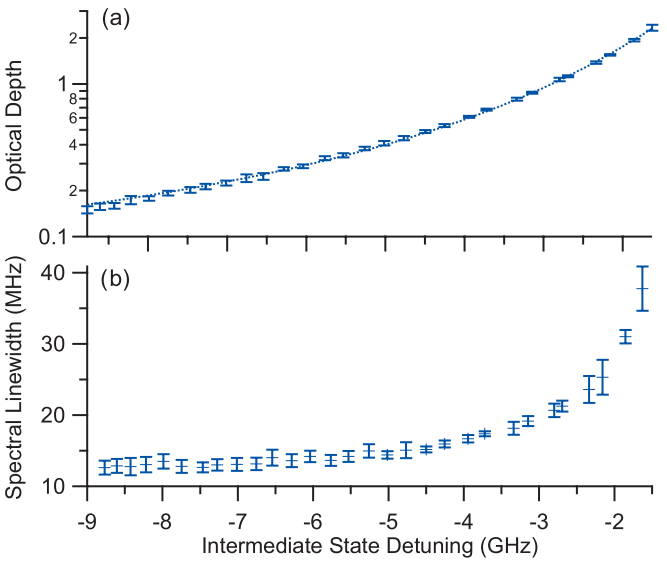


FIG. 4. (Color online) The two-photon transition's (a) optical depth $\alpha(0)$ (with fit) and (b) linewidth $\gamma_{\mathrm{FWHM}}$ as a function of intermediate state detuning ($\Delta_i$) where $P_{gi} \approx 60$ nW and $P_{ie} \approx 640$ $\mu$W.

upon single-photon detuning $\Delta_i$, as [1,10]

$$w(0) \propto \frac{P_{gi} P_{ie}}{\gamma_e\left(4\Delta_i^2 + \Gamma^2\right)}. \tag{2}$$

This is a Lorentzian line shape centered on the $|g\rangle \rightarrow |i\rangle$ transition frequency [1] with a width $\Gamma = \gamma_i$ being the linewidth of the intermediate state. However, when considering a thermal vapor, the Maxwell-Boltzmann velocity distribution naturally broadens this bandwidth. Furthermore, power dependent broadening of $\Gamma$ is expected [21] and was observed in the experiment. For optical powers of $P_{gi} \approx 60$ nW and $P_{ie} \approx 640$ $\mu$W, a Lorentzian fit to the data presented in Fig. 4(a) returned a two-photon excitation bandwidth FWHM of $\Gamma = 2.50 \pm 0.05$ GHz.

The second key characteristic for many applications is the dependence of two-photon absorption strength on input powers. A summary of this is shown in Fig. 5(a) for a detuning of $\Delta_i \approx 2$ GHz. The two-photon optical depth, defined using Eq. (2) as $\alpha(0) \propto w(0)/P_{gi}$, describes the absorption strength for sufficiently low optical powers where atomic saturation and optical pumping are negligible [10,20]. Atomic saturation was observed for $P_{gi} > 850$ nW and $P_{ie} > 500$ $\mu$W as seen in Fig. 5 by the combined reduction in absorption strength and increase in the spectral linewidth. A maximum two-photon optical depth of $\alpha(0) > 2.4$ [absorption $\mathscr{A}(0) > 90\%$] was observed for input powers of $P_{ie} \approx 870$ $\mu$W and $P_{gi} < 100$ nW.

Finally, for many applications the most important characteristic is minimizing the linewidth and decoherence of the two-photon transition. The behavior of the two-photon transition's linewidth $\gamma_{\mathrm{FWHM}}$ can be broken into two regions [1,10,14]:

$$\gamma_{\mathrm{FWHM}} = \begin{cases} \gamma_e + s\gamma_i\sqrt{1 + P_{gi}/P_{\mathrm{sat}}} & |\Delta_i| < \gamma_{\mathrm{Dop}} \\ \gamma_e & |\Delta_i| \gg \gamma_{\mathrm{Dop}}, \end{cases} \tag{3}$$

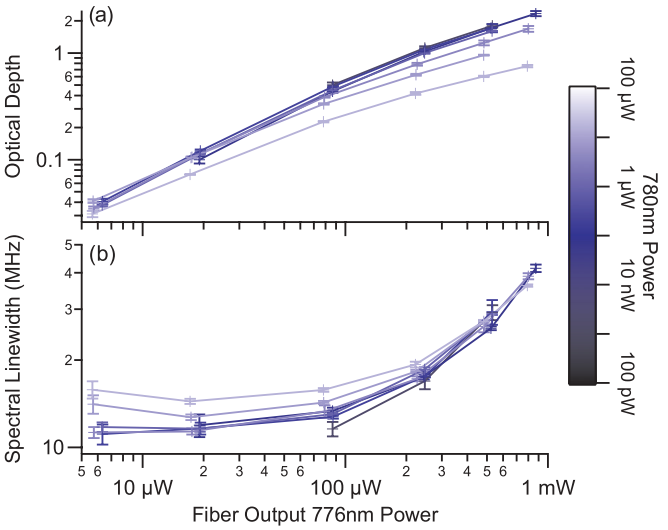


FIG. 5. (Color online) (a) Optical depth $\alpha(0)$ and (b) linewidth $\gamma_{\mathrm{FWHM}}$ dependence on laser powers where the intermediate state detuning is $\Delta_i \approx 2$ GHz.

where $s = (\omega_{gi} - \omega_{ie})/\omega_{gi}$, for this configuration $s \approx 0.005$, and $P_{\mathrm{sat}}$ is the transition's effective saturation power. It can be seen from Eq. (3) that when the lasers are resonant with the intermediate transition, the power broadened linewidth associated with the intermediate level contributes to the two-photon linewidth. This is confirmed experimentally in Fig. 4(b) where the linewidth expands for intermediate state detunings approaching $\gamma_{\mathrm{Dop}}$. In the limit that $|\Delta_i| \gg \gamma_{\mathrm{Dop}}$ the linewidth is seen to be constant as predicted from Eq. (3).

The linewidth was also seen to vary as a function of input power for a fixed frequency detuning, as shown in Fig. 5(b). In contrast to Eq. (3) and Fig. 4(b), the increase in two-photon spectral linewidth observed here is not induced by the intermediate state. Rather, it is the effect of inhomogeneous ac Stark shifts experienced by the atoms in different regions of the fiber's optical mode [9].

## V. ULTIMATE LINEWIDTH

The ultimate linewidth achieved was $10.4 \pm 0.5$ MHz, substantially broader than expected from the natural linewidth alone being 667 kHz [19]. Technical broadening mechanisms include intermediate level effects, light shifts, and laser noise. All were minimized below the resolution limit of the experiment. However, the effects of magnetic fields, residual Doppler, and transit-time broadening, could not be removed. Each of these effects are discussed below and their contribution summarized in Table I.

The effect of the intermediate level [as discussed in Eq. (3)] was minimized by driving the transition with a detuning of $\Delta_i \approx 3$ GHz. Optical powers were also minimized ($P_{gi} <$ 100 nW and $P_{ie} < 20$ $\mu$W), to ensure inhomogeneous light shifts did not broaden the spectral linewidth as shown in Fig. 5(b). Laser noise was minimized by stabilizing the ECDL to the reference optical cavity reducing frequency noise below the resolution limit of the experiment.

It was not feasible to shield the fiber from ambient magnetic fields due to the complexity of the vacuum system. An estimate of this broadening was determined by observing the two-photon linewidth while increasing the local magnetic field. Extrapolation of this data to the ambient field level provides an estimated ambient magnetic field broadening of $\approx 2.6 \pm 1.0$ MHz. Residual Doppler broadening is also present resulting in a contribution of 1.9 MHz $1/e$ half-width Gaussian broadening within the heated fiber. This was verified with identical measurements on a conventional macroscopic cell at room temperature.

TABLE I. Two-photon linewidth budget.

| | FWHM contribution (MHz) | |
|---|---|---|
| Broadening effect | Fiber | Cell |
| Natural linewidth [19] | 0.667 | 0.667 |
| Magnetic field | $2.6 \pm 1.0$ | $< 0.05$ |
| Residual Doppler[a] | $3.09 \pm 0.04$ | $2.79 \pm 0.02$ |
| Transit time[a] | $5.61 \pm 0.05$ | $< 0.1$ |
| Beam misalignment[a] | $< 0.01$ | $1.0 \pm 0.2$ |
| Convolved resultant | $10.1 \pm 0.4$ | $4.5 \pm 0.2$ |
| Experimental value | $10.4 \pm 0.5$ | $4.7 \pm 0.2$ |

[a]Theoretically calculated values based on measured temperature, mode area, and beam alignment.

The fiber core's confined geometry leads to transit-time broadening caused by short light-atom interaction times [22]. This effect was modeled using a four-level density matrix model which included a Maxwell-Boltzmann thermal velocity distribution which accounts for residual Doppler broadening; random atomic trajectories and the laser beam geometry [20] resulting in transit-time broadening; and splitting of the Zeeman sublevels which accounted for the observed magnetic field broadening. These effects were all convolved together to produce an expected spectral line shape. An estimate of the overlap of the counterpropagating modes within the fiber was measured by imaging the transmitted modes at both ends of the fiber. This showed an overlap region with diameter $13 \pm 1$ $\mu$m. Using this as the effective optical mode diameter, a transition spectra was generated from the model, which is shown in Fig. 3 to be in excellent agreement with the experimental data. As shown in Table I, the width of the modeled spectra is predicted to be $10.1 \pm 0.4$ MHz, which is consistent with the observed result.

In contrast, the reference cell was seen to have a linewidth of $4.7 \pm 0.2$ MHz as seen in Fig. 3. This is because the cell was magnetically shielded and the optical beam had a $1/e^2$ diameter of 1.3 mm causing negligible transit-time broadening. Minor misalignment between the 780- and 776-nm beams within the cell ($< 0.1^\circ$) caused additional Doppler broadening as indicated in Table I. This was avoided in the fiber due to its guidance properties.

To confirm transit-time broadening as the dominant effect within the fiber, and to rule out additional population relaxation processes, the excited state lifetime was directly observed through fluorescence decay measurements, shown in Fig. 6. If there are no other population relaxation mechanisms, the atomic fluorescence lifetime will be limited by the time of flight of the atoms across the fiber core. Observation of this fluorescence decay was enabled by rapidly switching off the excitation laser ($1/e$ falloff time of 55 ns). Analysis of the

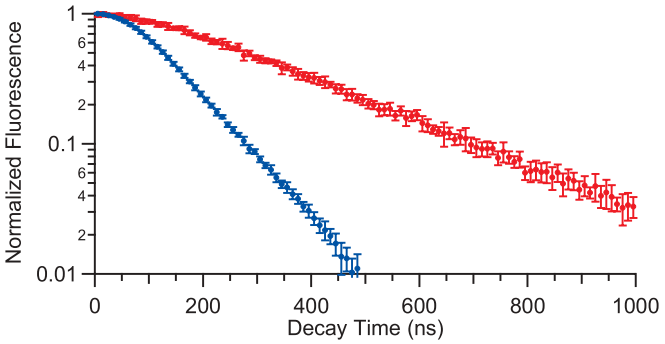


FIG. 6. (Color online) Fluorescence decay of the fiber (blue, lower) and cell (red, upper).

decay using methods described in [19] gave an excited state lifetime $\tau_l$ of $81 \pm 2$ and $226 \pm 8$ ns for the fiber and cell, respectively. The decay rate in the cell agrees with previous measurements (238 ns [19]). On the other hand, the fiber's excited state lifetime is shortened by 157 ns corresponding to a time of flight across the fiber core of $123 \pm 3$ ns using the formalism

$$\frac{1}{\tau_l} = \frac{1}{\tau_e} + \frac{1}{\tau_{tt}}, \tag{4}$$

where $\tau_e = 238$ ns is the natural lifetime of the excited state [19] and $\tau_{tt}$ is the transit time of the atoms across the fiber. This is consistent with a theoretical estimate of the expected time of flight across the fiber core of 132 ns, obtained by averaging over all possible velocities and trajectories. This agreement suggests that the dominant population relaxation process is from atom-wall collisions, ruling out other population relaxation mechanisms which could cause the observed broadening. Furthermore, the agreement confirms the earlier modeling underpinning the theoretical line shape (Fig. 3). Thus, this confirms that the limited transit time across the optical mode is the origin of the observed increased linewidth in the fiber.

## VI. CONCLUSION

We have demonstrated the ability to drive the $5S_{1/2} \rightarrow 5D_{5/2}$ two-photon transition within a Rb-filled HC-PCF. Even for very modest optical powers ($< 500$ $\mu$W) it is possible to obtain two-photon absorption depths close to 100%. Furthermore, it is possible to maintain this substantial absorption over large optical detunings $> 9$ GHz from the intermediate level. The ultimate linewidth of the two-photon transition was shown to be $10.4 \pm 0.5$ MHz, which is dominated by transit-time broadening and is consistent with theoretical modeling. Such narrow linewidths enable the two-photon excited state hyperfine splitting to be resolved.

## ACKNOWLEDGMENTS

The authors acknowledge financial support from the Australian Research Council under Grants No. DP0877938, No. DE120102028, No. FT0991631, and No. DP1094500. We are grateful to Francois Couny for his contribution in the fibre fabrication, and the Centre for Microscopy, Characterisation and Analysis at the University of Western Australia for use of the electron microscope.

[1] J. Bjorkholm and P. Liao, Phys. Rev. A **14**, 751 (1976).
[2] B. C. Jacobs and J. D. Franson, Phys. Rev. A **79**, 063830 (2009).
[3] D. A. Braje, V. Balić, G. Y. Yin, and S. E. Harris, Phys. Rev. A **68**, 041801(R) (2003).
[4] M. Bajcsy, S. Hofferberth, V. Balic, T. Peyronel, M. Hafezi, A. S. Zibrov, V. Vuletic, and M. D. Lukin, Phys. Rev. Lett. **102**, 203902 (2009).
[5] B. C. Jacobs, T. B. Pittman, and J. D. Franson, Phys. Rev. A **74**, 010303(R) (2006).
[6] J. D. Franson, B. C. Jacobs, and T. B. Pittman, Phys. Rev. A **70**, 062302 (2004).
[7] S. M. Hendrickson, M. M. Lai, T. B. Pittman, and J. D. Franson, Phys. Rev. Lett. **105**, 173602 (2010).
[8] L. Hilico, R. Felder, D. Touahri, O. Acef, A. Clairon, and F. Biraben, Eur. Phys. J.: Appl. Phys. **4**, 219 (1998).
[9] M. Poulin, C. Latrasse, D. Touahri, and M. Têtu, Opt. Commun. **207**, 233 (2002).
[10] M. Tanasittikosol, C. Carr, C. S. Adams, and K. J. Weatherill, Phys. Rev. A **85**, 033830 (2012).
[11] C. Perrella, P. S. Light, T. M. Stace, F. Benabid, and A. N. Luiten, Phys. Rev. A **85**, 012518 (2012).
[12] V. Venkataraman, K. Saha, P. Londero, and A. L. Gaeta, Phys. Rev. Lett. **107**, 193902 (2011).
[13] F. Nez, F. Biraben, R. Felder, and Y. Millerioux, Opt. Commun. **102**, 432 (1993).
[14] T. T. Grove, V. Sanchez-Villicana, B. C. Duncan, S. Maleki, and P. L. Goul, Phys. Scr. **52**, 271 (1995).
[15] F. Couny, F. Benabid, and P. S. Light, Opt. Lett. **31**, 3574 (2006).
[16] B. Stoicheff and E. Weinberger, Phys. Rev. Lett. **44**, 733 (1980).
[17] K. H. Weber and K. Niemax, Opt. Commun. **31**, 52 (1979).
[18] P. Siddons, C. S. Adams, C. Ge, and I. Hughes, J. Phys. B **41**, 155004 (2008).
[19] D. Sheng, A. Pérez Galván, and L. A. Orozco, Phys. Rev. A **78**, 062506 (2008).
[20] T. M. Stace and A. N. Luiten, Phys. Rev. A **81**, 033848 (2010).
[21] R. Salomaa, J. Phys. B **10**, 3005 (1977).
[22] M. Bruvelis, J. Ulmanis, N. N. Bezuglov, K. Miculis, C. Andreeva, B. Mahrov, D. Tretyakov, and A. Ekers, Phys. Rev. A **86**, 012501 (2012).